Title: Numerical and experimental study of mechanisms involved in boiling histotripsy

Author names and affiliations: Ki Joo Pahk[1,*], Pierre Gélat[1], David Sinden[2], Dipok Kumar Dhar[3] and Nader Saffari[1]

[1]Department of Mechanical Engineering, University College London, London, WC1E 7JE, UK

[2]Acoustics Group, National Physical Laboratory, Teddington, TW118UQ, UK

[3]Institute for Liver and Digestive Health, Royal Free Hospital, University College London, London, NW3 2PF, UK

[*]Now at Center for Bionics, Biomedical Research Institute, Korea Institute of Science and Technology (KIST), Seoul, 02792, Republic of Korea

Corresponding author:

Nader Saffari

Department of Mechanical Engineering, University College London, Torrington Place, London, WC1E 7JE, United Kingdom

E-mail: n.saffari@ucl.ac.uk

Tel: +44(0)2076797180

Abstract

The aim of boiling histotripsy is to mechanically fractionate tissue as an alternative to thermal ablation for therapeutic applications. In general, the shape of a lesion produced by boiling histotripsy is tadpole like, consisting of a “head” and a “tail”. While a number of studies have demonstrated the efficacy of boiling histotripsy for fractionating solid tumours, the exact mechanisms underpinning this phenomenon are not yet well understood, particularly the interaction of a boiling vapour bubble with incoming incident shockwaves. To investigate the mechanisms involved in boiling histotripsy, a high-speed camera with a passive cavitation detection (PCD) system were used to observe the dynamics of bubbles produced in optically transparent tissue mimicking gel phantoms exposed to the field of a 2.0 MHz High Intensity Focused Ultrasound (HIFU) transducer. We observed that boiling bubbles were generated in a localised heated region and cavitation clouds were subsequently induced ahead of the expanding bubble. This process was repeated with HIFU pulses and eventually resulted in a tadpole shaped lesion. A simplified numerical model describing the scattering of the incident ultrasound wave by a vapour bubble was developed to help interpret the experimental observations. Together with the numerical results, these observations suggest that the overall size of a lesion induced by boiling histotripsy is dependent upon the sizes of (a) the heated region at the HIFU focus and (b) the backscattered acoustic field by the original vapour bubble.

Keywords: high intensity focused ultrasound, boiling histotripsy, boiling bubbles, cavitation clouds.

INTRODUCTION

High intensity focused ultrasound (HIFU) is a non-invasive ultrasound technique which has been used to thermally necrose solid tumours without disruption to surrounding tissue (ter Haar and Coussios 2007; Aubry et al. 2013). In recent years, an alternative HIFU technique to thermal ablation has been developed. This is known as mechanical tissue fractionation or histotripsy. Acoustic peak positive (P_+) and negative (P_-) pressures at the HIFU focus used in histotripsy are comparable to those in the shockwaves used in lithotripsy for kidney stone fragmentation (Zhu et al. 2002; Pishchalnikov et al. 2003). One of the initial works to show the feasibility of using acoustic shock waves to induce controlled mechanical injuries in soft tissue was published in 1997 (Tavakkoli et al. 1997). A well-defined lesion in the form of a cavity can be produced by histotripsy without any significant thermal damage at the periphery of the cavity. Recent *in vivo* studies on kidney, prostate, heart and liver have shown that a lesion produced by histotripsy contains complete fragmentation of tissue and is sharply demarcated between treated and untreated regions (Roberts et al. 2006; Hall et al. 2009; Styn et al. 2010; Xu et al. 2010; Vlaisavljevich et al. 2013; Khokhlova et al. 2014; Pahk et al. 2015, 2016). Subcellular debris remaining inside a mechanically fractionated lesion can be absorbed as part of the physiologic healing mechanism, whereas a thermally ablated lesion becomes fibrous scar tissue (Hoogenboom et al. 2015).

In histotripsy, there are two different methods of creating pure mechanical damage of soft tissue by (a) pulsed ultrasound cavitation or (b) shock wave heating and millisecond boiling (Parsons et al. 2006; Canney et al. 2010a, 2010b; Maxwell et al. 2011; Khokhlova et al. 2011, 2014; Khokhlova et al. 2015). In both methods, acoustic cavitation is believed to be one of the main mechanisms for inducing mechanical tissue fractionation (Khokhlova et al. 2015). An inertial cavitation cloud at the HIFU focus can be formed by two different mechanisms, termed shock scattering histotripsy and intrinsic threshold histotripsy (Allen and

Hall 2015; Vlaisavljevich et al. 2016). For shock scattering histotripsy, a number of microsecond-long HIFU pulses with high peak positive ($P_+ > 80$ MPa) and negative ($P_- = 15 – 25$ MPa) acoustic pressures at the focus are used to produce a dense bubble cloud. This cloud formation results from the production of a greater peak negative pressure field generated by the interference between the reflected and inverted peak positive pressure from a single cavitating bubble and the incoming incident rarefactional phase (Maxwell et al. 2011; Vlaisavljevich et al. 2014). In intrinsic threshold histotripsy, a single microsecond-long HIFU pulse with a single dominant negative pressure P_- of 24 – 30 MPa at the focus is employed to induce a cavitation cluster directly from the negative pressure phase of the incident acoustic wave (Lin et al. 2014; Maxwell et al. 2013; Vlaisavljevich et al. 2015a, 2015b). Because the pressure threshold for cavitation clouds is –28 MPa for most soft tissues (Maxwell et al. 2013; Lin et al. 2014), the site of the bubble cloud is spatially confined to the HIFU focus.

In contrast to shock scattering or intrinsic threshold histotripsy, there is another method of inducing a mechanically fractionated lesion. This ultrasound technique is known as boiling histotripsy, which utilises shock wave heating to produce a boiling vapour bubble (as opposed to cavitation clouds) and fractionate soft tissue with a number of millisecond HIFU pulses (Khokhlova et al. 2015). Boiling histotripsy has been demonstrated in *ex vivo* bovine liver (Khokhlova et al. 2011, Wang et al. 2013), heart (Wang et al. 2013), kidney (Schade et al. 2014) and *in vivo* porcine and rat liver (Khokhlova et al. 2014; Pahk et al. 2015, 2016). These studies have shown that boiling histotripsy can induce similar lesions to those generated by shock scattering histotripsy or intrinsic threshold histotripsy.

Mechanisms involved in boiling histotripsy are currently being investigated by several research groups such as Canney et al. (2010a), Kreider et al. (2011), Khokhlova et al. (2011), Wang et al. (2013) and Simon et al. (2012, 2015). In soft tissue, significant acoustic wave distortion at the HIFU focus due to tissue nonlinearity leads to the production of a shock

wavefront. This wavefront contains tens of higher order harmonic components of the fundamental frequency. Since the absorption of ultrasound energy in tissue increases with frequency (ter Haar and Coussios 2007), a shockwave enables the heating rate to be dramatically increased. Canney et al. (2010a) demonstrated that localised heating by shockwaves at the HIFU focus can raise tissue temperature to 100^{o}C in a few milliseconds followed by the formation of a boiling vapour bubble at the HIFU focus. This bubble then grows to millimetre size, which may tear off tissue due to shear stresses produced around the oscillating bubble (Khokhlova et al. 2011). The growth of this millimetre-sized bubble, known as rectified bubble growth, is likely to be due to the combination of the asymmetry in the compressional and rarefactional pressure phases in the shock waveforms and water vapour transport (Kreider et al. 2011). After the formation and explosive growth of a boiling bubble, it further interacts with incoming incident shockwaves to promote a mechanical tissue fractionation process (Maxwell et al. 2012). A miniature acoustic fountain and atomisation may occur at the tissue-bubble interface to emit jetting with sub-micrometre sized tissue fragments into the bubble (Simon et al. 2012).

In general, the shape of a lesion produced by boiling histotripsy is tadpole like, consisting of a “head” and a “tail” with the “head” closest to the HIFU source (Khokhlova and Hwang 2011). Canney et al. (2010b) and Khokhlova et al. (2011) observed that the HIFU focus was at the “tail” and the “head” migrated towards the HIFU transducer during the course of boiling histotripsy. Khokhlova et al. (2011) and Simon et al. (2012) suggested that the production of a “head” shaped lesion is likely to be due to the formation of a boiling bubble at the HIFU focus and the HIFU atomisation at the tissue-bubble interface. Besides this, the “tail” of a lesion may be formed by streaming of the liquefied tissue within the forming “head” (Wang et al. 2013). These proposed mechanisms, however, are not enough to explain the prefocal shift of the lesion “head” towards the transducer, because the atomisation

process is likely to be limited to the region where shocks and boiling bubbles are present (Khokhlova et al. 2011, Wang et al. 2013). Therefore, there may be other mechanisms involved in boiling histotripsy besides the HIFU atomisation and the streaming effects.

While a number of studies have demonstrated the efficacy of boiling histotripsy for fractionating tumours, the exact mechanisms underpinning this phenomenon are poorly understood, particularly the interaction of a boiling bubble with incoming incident shockwaves. To that end, the main objective of the present study is to help provide a better understanding of the mechanisms behind the formation of a mechanically induced tadpole shaped lesion resulting from boiling histotripsy. In this study, a high-speed camera and a passive cavitation detection (PCD) system are used to observe the dynamics of bubbles induced in tissue mimicking gel phantoms exposed to HIFU fields and record the corresponding acoustic emissions. Furthermore, a numerical model describing the incidence of ultrasonic waves on a vapour bubble close to the focus of the HIFU transducer and the backscattered field by the bubble, is developed using a boundary element method (BEM).

MATERIALS AND METHODS

HIFU experimental arrangement

A schematic diagram of the experimental set up used in this study is shown in Figure 1. The experiment was performed in an acrylic water bath filled with degassed and de-ionised water at a temperature of 20^{o}C. A water treatment system (Precision Acoustics Ltd, Dorset, UK) was used for degassing. A 2.0 MHz single element bowl-shaped HIFU transducer (Sonic Concepts H106, Bothell, WA, USA) with an aperture size of 64 mm, a focal length of 62.6 mm, and lateral and axial full width half maximum (FWHM) pressure dimensions of 1.05 mm and 6.67 mm was used. The HIFU transducer was characterised in our previous study (Pahk et al. 2016) using a calibrated 0.2 mm polyvinylidene fluoride (PVDF) needle

hydrophone (Prevision Acoustics Ltd, Dorchester, UK) in water (free-field) under linear propagation conditions. The HIFU source was driven by a function generator (Agilent 33220A, Santa Clara, CA, USA) via a linear radiofrequency (RF) power amplifier (ENI 1040L, Rochester, NY, USA). A computer with waveform generation software (Agilent Waveform Builder, CA, USA) was used for driving the function generator with the desired HIFU pulsing protocol. A power meter (Sonic Concepts 22A, Bothell, WA, USA) was connected between the RF power amplifier and the HIFU source to measure the level of the electrical power P_{elect} supplied to the transducer.

During the experiments, the position of the HIFU transducer was fixed relative to the phantom in the water bath and an acoustic absorber (Precision Acoustics Ltd AptFlex F28, Dorchester, UK) was placed on the opposite end to minimise ultrasonic reflections. A 10 MHz focused PCD (20 mm in diameter and 64 mm in geometric focal length, Sonic Concepts Y107, Bothell, WA, USA) featuring a wide bandwidth (10 kHz–20 MHz) was connected to a digital oscilloscope (LeCroy HDO 6054, Berkshire, UK). This PCD was used to obtain acoustic emissions resulting from cavitation activity at the HIFU focus. A sampling frequency of 0.5 GHz was used.

Tissue mimicking gel phantoms

An optically transparent tissue mimicking phantom containing a polyacrylamide gel with bovine serum albumin (BSA) used in this study has also been used in a number of other boiling histotripsy studies (Canney et al. 2010a; Khokhlova et al. 2011; Zhou and Gao 2013). Temperatures above 60^{o}C cause BSA protein to denature and form an opaque thermal lesion, which can be visualised. Table 1 shows the chemical composition required to produce a 50 mL gel with 7% BSA concentration. A tissue phantom consisting of the chemical composition listed in Table 1 has very similar acoustic and thermal properties to those of liver, except for

the attenuation coefficient, which is 0.15 dB $cm^{-1}MHz^{-1}$ rather than that for liver which is 0.52 dB $cm^{-1}MHz^{-1}$ (Lafon et al. 2005; Khokhlova et al. 2011).

The tissue phantom was prepared by first mixing 3.5 g of BSA (Sigma-Aldrich A7906, Dorset, UK) in 35.805 mL of degassed and de-ionised water. The mixture was gently stirred to dissolve the BSA completely. The solution was then placed in a vacuum chamber (Edwards High Vacuum ISC30A, Sussex, UK) and held in a vacuum of 720 mm Hg for 30 minutes for additional degassing. 8.75 mL of acrylamide (Sigma-Aldrich A9926, Dorset, UK) was added to the mixture followed by a 1 mol L^{-1} TRIS buffer (Sigma-Aldrich T2694, Dorset, UK) and a 0.42 mL of APS (Sigma-Aldrich A7460, Dorset, UK) to initiate polymerisation. Because acrylamide is a neurotoxic substance, the mixing process was performed in a fume hood (Labcaire T400L, Somerset, UK) with appropriate safety measures. The entire solution was again stirred gently and placed in the vacuum chamber with a vacuum of 720 mm Hg for 1 hour. 0.025 mL of TEMED (Sigma-Aldrich T9281, Dorset, UK) was finally added to the solution to accelerate the polymerisation process. The final solution was immediately poured into a customised mould (6 × 6 × 6 cm). Because the polymerised gel has a limited lifespan of several weeks (Khokhlova et al. 2006), it was stored in an air-tight plastic bag at 8^{o}C and used the next day for experiments.

Prior to the camera experiments, the tissue phantom was kept at room temperature until its temperature reached 20^{o}C. The phantom was then cut into cuboid samples (1.5 × 3 × 6 cm) and clamped in a custom-built holder (4.5 × 5 × 7.5 cm). The holder coupled with the phantom was attached to a customised three-axis positioning system for alignment with the HIFU focus. The distance from the centre of the transducer surface to the phantom was 57.6 mm. Therefore, the HIFU focus was 5 mm below the surface of the phantom. This depth was chosen according to our previous *in vivo* study (Pahk KJ et al. 2016) that shows the production of a well-defined ‘tadpole’ shaped lesion at 5 mm below the surface of the liver

without rupturing the liver surface. 17 tissue phantoms in total (n = 17) were used in this study.

Camera set up

A high speed camera (FASTCAM-ultima APX, Photron, San Diego, CA, USA) with a 12X Navitar lens (Navitar, Rocester, NY, USA) connected to a three-axis-positioning system (Sherline Products 5430, Vista, CA, USA) was used to film the bubble dynamics induced at the HIFU focus in the tissue phantom. The camera was operated at 1000, 15,000 and 100,000 frames per second (fps) with a shutter speed of 1/1000 s, 1/15000 s and 1/100000 s, and a pixel resolution of 512 × 128, 1028 × 128 and 128 × 32, respectively (24 μm/pixel). During the experiments, 15,000 and 100,000 fps were used to capture bubble dynamics induced by a single or five HIFU pulses in the gel whilst 1,000 fps was employed for fifty HIFU pulses due to memory limitation. All experiments were backlit with an illuminating system (Solarc ELSV-60, General Electric Company, Connecticut, USA). Hence, captured optical images appeared as shadowgraphs where the tissue phantom appeared grey and HIFU-induced bubbles appeared black. Optical images were post-processed with Photron FASTCAM Viewer (Photron, San Diego, CA, USA). Tissue phantoms were cross-sectioned after HIFU exposure for morphological analysis.

During the experiments, a camera processor (FASTCAM-ultima APX, Photron, San Diego, CA, USA) triggered the camera and the function generator at the same time to synchronise the image capturing process and HIFU exposure.

HIFU exposure condition

A 10 ms-long HIFU pulse with P_{elect} = 200 W (nominal electrical to acoustic power conversion efficiency of 85%, P_+ = 85.4 MPa and P_- = –15.6 MPa) was used to produce a

lesion in the tissue phantom. The duty cycle (1%) and the pulse repetition frequency (1 Hz) were kept constant while changing the number of pulses, which was set to 1, 5 or 50. In boiling histotripsy, it has been shown that the time to initiate boiling at the HIFU focus can be reliably predicted theoretically (Canney et al. 2010a; Khokhlova et al. 2011; Wang et al. 2013). Acoustic peak positive (P_+) and negative (P_-) pressures at the HIFU focus in the gel were, therefore, obtained by numerically solving the Khokhlov-Zabolotskaya-Kuznetsov (KZK) parabolic nonlinear wave propagation equation for a set of input parameters using the HIFU Simulator v1.2 (Soneson 2009). The simulated acoustic waveform at the focus is shown in Figure 2(a). Figure 2(b) depicts the corresponding peak temperature rise. This was calculated using the bioheat transfer (BHT) equation (Pennes 1948) and the time to reach the boiling temperature of 100^{o}C (t_b) was predicted to be 3.66 ms. The physical properties of the tissue phantom used in the simulations are listed in Table 2. The HIFU exposure parameters used in this study were verified for the creation of a cavity with *in vivo* experiments reported earlier (Pahk et al. 2015, 2016) and were similar to those used by Khokhlova et al. (2011).

Scattered pressure fields

The presence of a vapour bubble close to the focus of the HIFU transducer is likely to cause scattering of the incident ultrasonic field due to the difference in the acoustic impedance between water vapour and the tissue phantom. This phenomenon may lead to constructive and destructive interactions of the scattered field with the incident field, potentially generating localised peak negative pressures, leading to additional cavitation nucleation sites. Furthermore, the presence of a vapour bubble close to the transducer focus may also lead to a distortion of the focus and generate a shadow zone.

It is well-known that the KZK equation can only simulate one-way par-axial propagation. Producing a full-wave nonlinear acoustic propagation model capable of dealing

with scattering by localised heterogeneities remains a challenge. This is particularly the case if the computational domain is large relative to the wavelength of the highest frequency present in the ultrasonic signal. On the basis of the KZK simulations, significant harmonic content is present at the focus up to 10 MHz. This is likely to result in a densely meshed computational grid. It is, therefore, likely that accurately modelling such a configuration will present substantial computational challenges. To get a qualitative appreciation of what the effects of scattering of the incident HIFU field by a vapour bubble may be, a linear scattering analysis was, therefore, opted for. The calculated scattered acoustic pressure fields based upon the linearity assumption would therefore only be for qualitative analysis. Boundary element methods (BEM) are particularly well-suited to dealing with exterior scattering problems, and such analysis techniques will be opted for here. In BEM, the partial differential equation to be solved is reformulated into an integral equation that is defined on the boundary of the domain (in this case, on the surface of the vapour bubble) and an integral that relates the boundary solution to the solution at any point in the domain. The boundary integral equation may then be solved by discretising the surfaces defined by the domain boundaries into smaller regions known as boundary elements. A major advantage of BEM over other numerical schemes, such as finite difference time domain methods, is that the discretisation occurs only over the surfaces rather than over the entire domain. More details on BEM are provided by Banerjee (1994).

The BEM implementation used in this study was described by Gélat et al. (2014, 2015). The method is a colocation BEM implementation of the Kirchhoff-Helmholtz integral equation, which uses isoparametric elements with quadratic shape functions. The scatterer is assumed to be locally reacting so that $\partial p/\partial n = i\omega\rho_v u_n$ on the surface of the vapour bubble, where p is the acoustic pressure in the liquid, n is the node on the mesh of the surface, u_n is the normal component of the particle velocity vector, ρ_v is the liquid density, ω is the angular

frequency and $i^2 = -1$. Transmission of acoustic waves through the bubble was neglected, due to the large difference between the acoustic impedance of water vapour and that of the tissue phantom (Canney et al. 2010a).

For computation of scattered acoustic fields from a boiling bubble, the BEM scheme requires an incident acoustic pressure field on the surface of the scatterer as input data. This was derived using a Rayleigh integral method (Pierce 1989) by effectively discretising the surface of the HIFU source into smaller surfaces with a point source located at their centroid. By weighting each source with the appropriate surface area and by summing all their contributions, the incident field at any required location may be computed. This is achieved through a discretisation of the following integral

$$p(\vec{r},t) = \frac{i\rho ck}{2\pi} e^{i\omega t} \iint_s \frac{e^{-ik\|\vec{r}-\vec{r}_0\|}}{\|\vec{r}-\vec{r}_0\|} \vec{u}\cdot\vec{n}\,dS$$

where ρ is the density of the tissue phantom, $k = \omega/c$ is the acoustic wave number and c is the sound speed in the phantom. $\vec{r}$ depicts a position vector in the acoustic domain, $\vec{r}_0$ a position on the surface of the source, $\vec{n}$ is the unit normal vector on the surface of the source (pointing towards to the focus), $\vec{u}$ is the velocity and s is the radiating surface of the HIFU source, which is assumed to be moving uniformly in the radial direction.

The exterior domain was assumed to be homogeneous, possessing the properties of the tissue phantom gel. In fact, this domain also comprises a region of water between the HIFU source and the gel. This water region was not included here, and the normal surface velocity of the transducer was adjusted to result in 22 MPa at the focus, in the absence of the scatterer. The pressure value of 22 MPa was obtained from the simulated acoustic pressure for the first harmonic using the KZK simulation (i.e., in the linear case). The resulting acoustic pressure at focus is shown in Figure 3(b), which represents the sum of the incident and the scattered pressure magnitude from a vapour bubble.

RESULTS

The formation of a boiling bubble in the tissue phantom gel with a single HIFU pulse

Figure 4 shows a sequence of camera images obtained over a single 10 ms HIFU pulse in the tissue mimicking gel phantom with an acoustic power of 170 W (P_+ = 85.4 MPa; P_- = –15.6 MPa at the HIFU focus). Localised heating in the HIFU focal region is observed as a dark elliptical shape at 3.4 ms (Figure 4(b)). This heated region corresponds well to the simulated temperature contour plot shown in Figure 4(c). A large bubble of 360 μm in diameter appears in this heated region after 3.6 ms of exposure to the HIFU field (indicated by an arrow in Figure 4(d)). This bubble is hereafter referred to as a boiling bubble because its onset time matches the calculated time to reach a boiling temperature of 100°C (t_b = 3.66 ms) (Khokhlova et al. 2011). A significant increase in the PCD voltage occurs as this large boiling bubble manifests itself. This can be seen in the PCD voltage vs time plot in Figure 5(a). Also coinciding with the appearance of this bubble is the manifestation of higher order multiple harmonic components of the fundamental frequency (2 MHz) in the spectrogram in Figure 5(b). These significant changes are indications of the formation of a boiling bubble due to the reflection of an incident nonlinear-shocked wave from this bubble (Canney et al. 2010a).

During the experiments, the time to boiling for the single HIFU pulse in the gel was 3.78 ± 0.67 ms (mean ± standard deviation SD with n = 17) with differences of 0.12 ms between the PCD measurement and the temperature simulation.

After the formation of a boiling bubble at t = 3.6 ms (see Figure 4(d)), a cavitation cluster is subsequently produced in front of the boiling bubble, progressing towards the HIFU source until the HIFU pulse is switched off (see Figures 4(e) to (h)). Simultaneously with the generation of the bubble cloud, significant appearance of broadband emissions (an indicator of inertial cavitation) is noticed within the black dashed lines in the corresponding spectrogram plotted in Figure 5(b). In addition to the generation of a cavitation cluster, a

secondary localised heated region at ~1 mm away from the primary boiling bubble further along the beam axis is observed. This event is indicated by an arrow in Figure 4(e) and is followed by the production of a secondary boiling bubble at t = 5.7 ms, also indicated by an arrow in Figure 4(f). More boiling bubbles can be seen to form at t = 7.6 ms towards the primary boiling bubble (see Figure 4(g)). These secondary boiling bubbles are spatially confined to the localised heated region.

The formation of a tadpole shaped lesion with multiple HIFU pulses

Five HIFU pulses

Figure 6 shows a series of high speed camera images taken during five 10 ms HIFU pulses. Images in the left column represent the formation of a boiling bubble during each HIFU pulse (indicated by arrows in Figure 6(a)), whereas those in the middle column show bubble activities at the end of each HIFU pulse (see Figure 6(b)). During each HIFU pulse, a boiling bubble appears either at the HIFU focus or close to the focus (within 1 mm, see Figure 6(a)), but disappears in the time interval between HIFU pulses (1% duty cycle). The time taken to form a boiling bubble decreases with HIFU pulses (3.6, 3.1, 2.9, 2.5 and 2.3 ms). Besides this boiling bubble, a cavitation bubble clouds is always produced in front of a boiling bubble (indicated by the blue arrows in Figure 6(b)), persisting throughout each HIFU exposure, but disappearing between HIFU pulses.

The corresponding induced mechanical damage in the gel prior to the arrival of the next HIFU pulse is shown in the right column in Figure 6(c). Examining the phantom morphology at the HIFU focus, residual mechanical damage of the gel is optically visible and the size of the lesion becomes enlarged with the number of HIFU pulses. When comparing the location of the bubbles (i.e. boiling bubbles and cavitation clouds) with the corresponding residual damage induced in the phantom (see Figures 6(b) and (c)), the position of the “head” shaped

lesion corresponds well to that of the cavitation cloud, whereas the boiling bubbles generated in the heated region match the location of the "tail" shaped lesion. In addition, bubbles less than 200 μm in diameter are pushed away from the HIFU focus (indicated by the black arrows in Figure 6(b)) most probably due to the HIFU radiation force. This movement may also contribute to the formation of the "tail" together with the generation of boiling bubbles.

Fifty HIFU pulses

In boiling histotripsy, 10 to 50 HIFU pulses are usually delivered to produce a well-defined mechanically fractionated lesion (Maxwell et al. 2012). Figure 7 shows a number of high speed images captured during 50 HIFU pulses. The shape of a tadpole-like mechanical damage produced in the phantom corresponds well to the locations of a cavitation cloud and of boiling bubbles, in the "head" and in the "tail", respectively. This is further confirmed by cross sectioning the lesion immediately after exposure to the 50^{th} HIFU pulse, as shown in Figures 7(f) and (g). No evidence of thermal damage, which would manifest itself as an opaque lesion (Khokhlova et al. 2011), was present.

Figure 8 shows the length along the direction of wave propagation and the width in the lateral direction of the "head" and of the "tail" as a function of the HIFU pulse numbers. After the fifth HIFU pulse, the length of the "head" does not increase significantly, whereas the width of the "head" and both the width and length of the "tail" continue to grow. After the 30^{th} HIFU pulse, the overall lesion size does not change significantly.

DISCUSSION

Formation of a boiling bubble

In this work, the mechanism for the formation of a tadpole shaped lesion produced by boiling histotripsy was investigated both experimentally and numerically. Canney et al. (2010a) and

Khokhlova et al. (2011) showed that localised shock wave heating can increase the temperature to 100^{o}C in a few milliseconds followed by the formation of a boiling vapour bubble at the HIFU focus. The experimental results presented in this study concurred with theirs. A boiling bubble appeared in a localised heated region (see Figure 4). The boiling time resulting from a single 10 ms HIFU pulse in the gel (3.78 ± 0.67 ms, mean ± SD with n = 17) agreed well with that obtained from the temperature simulation, where the computed time to boil was predicted to be 3.66 ms. Furthermore, it was noticed that the onset time of a boiling bubble reduced with the number of HIFU pulses used (see Figure 6). This is most likely to be due to an accumulation of heat at the HIFU focus, where the peak temperature does not return to ambient temperature between pulses (Khokhlova et al. 2011; Zhou and Gao 2013).

During the course of HIFU exposure, the changes in temperature dependent acoustic properties, especially speed of sound, can lead to a shift of the HIFU focus in the axial direction towards the transducer (Hallaj et al. 2001). In Figures 4(d) and 6(a), it can be seen that a boiling bubble forms at the edge of the heated region during the first 10 ms HIFU pulse. This was also observed by Khokhlova et al. (2011). In the presence of a localised region heated by shockwaves, there is a large temperature gradient across the edge of the region. This eventually leads the local speed of sound in the heated volume to be greater than that outside of this region, causing an acoustic refraction effect at the interface.

Interaction of a boiling bubble with an incident shockwave

Maxwell et al. (2011) showed that the reflection and inversion of incident shockwaves from the surface of a single cavitating bubble produces a large peak negative pressure field, leading to additional bubble nucleation sites for cavitation clouds. This phenomenon is known as the shock scattering effect. This cavitation cluster was also observed during the course of boiling histotripsy, after the creation of a boiling bubble at the HIFU focus (see Figures 4(e)-(h)).

Simultaneously with the bubble cloud formation in front of a boiling bubble, a secondary localised heated region appears within the HIFU focal region followed by a secondary boiling bubble (see Figures 4(e),(f)). This is likely to be due to (a) the fact that the incident acoustic field is partially shielded by the cavitation cluster together with the boiling bubble and (b) the larger size of the HIFU focal width (FWHM of 1.05 mm) relative to that of the region heated by shocks (~0.2 mm, see Figure 4(c)). Indeed, as a result of the constructive and destructive interference between the incident field and that scattered by the secondary boiling bubble, local pressure minima as well as enhanced heating may be induced. This may lead to the generation of a number of boiling bubbles in front of the secondary boiling bubble moving towards the transducer (see Figures 4(f)-(h)). Figure 9 shows the simulated sum of the incident pressure and the pressure scattered by a boiling vapour bubble. The backscattered acoustic pressure field in front of the bubble and the reduced acoustic pressure in the shadow zone behind the bubble can be clearly observed. The boundary element numerical results have been obtained based on the linearity assumption. So although both the backscattered acoustic field and the field behind the bubble are given by the simulations, it is only the pressure field behind the bubble that can be used for a direct comparison with the experimental observations. This is because the dominant components in the backscattered field of an incident shock from a bubble have been experimentally observed to be the higher frequency components (Maxwell et al. 2012). The linear model used here does not model a shock or the higher harmonics of the fundamental. The fundamental component, which is the only component modelled here, and the lower frequency harmonics in a shock are however expected to be scattered more weakly and thus more in the forward direction, i.e. behind the bubble. Therefore behind the first large vapour bubble, the simulated field can be expected to be more accurate and thus used to explain the occurrence of the secondary boiling vapour bubbles within the HIFU focal zone.

Mechanisms for the creation of a tadpole shaped lesion

Khokhlova et al. (2011), Simon et al. (2012) and Wang et al. (2013) proposed that the formation of a tadpole shaped lesion produced by boiling histotripsy is most likely to be due to the explosive growth of a boiling bubble together with the HIFU atomisation for a "head" shaped lesion and the streaming of a mechanically fractionated tissue within the forming "head" for a "tail" shaped lesion. The experimental results presented in this study, however, could possibly support an additional mechanism being responsible for the formation of a tadpole shaped lesion. The mechanical destruction of the polymer structure of the tissue phantom corresponded well to the locations of cavitation clouds for a "head" and boiling bubbles for a "tail", respectively (see Figures 6 and 7). The shape of the lesion was further confirmed by cross sectioning it immediately after the HIFU insonation (see Figures 7(f) and (g)). Based upon the numerical and experimental results presented in this work, another possible mechanism for the formation of a "tadpole" shaped lesion resulting from boiling histotripsy is proposed. This is shown in Figure 10. After the formation and explosive growth of a boiling bubble at the HIFU focus, the shock scattering effect leads to the production of inertial cavitation clouds (i.e. violent bubble collapses) in front of the boiling bubble. These bubble clouds, which are known to be responsible for shock scattering histotripsy and intrinsic threshold histotripsy (Maxwell et al. 2012; Khokhlova et al. 2015), enable the disruption of tissue (Lake et al. 2008; Hall et al. 2009; Schade et al. 2012a, 2012b; Vlaisavljevich et al. 2013) leading to the production of the "head" of the lesion. In addition to this, the shear stresses produced around a number of boiling bubbles within a localised heated region (Khokhlova et al. 2011) may create the "tail" of the lesion. Simultaneously, ultrasonic atomisation at the tissue-bubble interface may also contribute to some extent to the production of the "tail" of the lesion; however, this process is spatially limited by the presence of shocks with high enough pressure amplitudes to cause tissue atomisation

(Khokhlova et al. 2011, Wang et al. 2013). Cavitation clouds which form right in front of the vapour cavity may weaken the tissue or gel to facilitate ultrasonic atomisation process (Khokhlova et al. 2011).

The variation of the size of a lesion with the number of HIFU pulses

As shown in Figures 7 and 8, the overall size of the lesion produced by boiling histotripsy increased gradually with the number of HIFU pulses, but did not change significantly starting from the 30^{th} pulse with the HIFU exposure condition used in this study. Khokhlova et al. (2011) and Wang et al. (2013) have also observed a similar trend in the growth of a lesion size with HIFU pulses. With the proposed mechanism described in Figure 10, it is suggested that the change of a lesion dimension is primarily dependent upon the extent of a localised heated region and the pressure amplitude of backscattered acoustic fields. As a heated region broadens with an increase in the number of HIFU pulses due to the accumulation of heat, more boiling bubbles with larger sizes will form within this heated volume. These spatially confined boiling bubbles lead to the formation of a tail for the lesion which grows in both axial and lateral directions along the beam axis. Simultaneously, the enlarged boiling bubble with a larger surface area generates a wider backscattered acoustic field (see Figure 11). This results in the formation of a wider cavitation cluster in the lateral direction towards the HIFU source, producing a wider head for the lesion. However, as heat transfer processes reach equilibrium in between HIFU pulses, the volume over which the heating occurs reaches a maximum (Wang et al. 2013). It is, therefore, reasonable to assume that beam width of the backscattered pressure field also reaches a maximum. As a result of this, the axial and lateral sizes of a “tail” do not change and neither does the lateral size of a “head”. Furthermore, the reduction of the pressure amplitude of backscattered fields due to attenuation limits the axial growth of a “head” towards the HIFU source. Cavitation clouds, for example, stop

progressing in the direction of the HIFU transducer when the sum of incident and scattered acoustic pressures is below a pressure threshold for cavitation clouds, which is –28 MPa for most soft tissues (Maxwell et al. 2013; Lin et al. 2014). This is the most likely reason why cavitation clouds were not optically observed at the surface of the phantom in the course of boiling histotripsy whereby the axial extent of the resulting lesion did not rupture the surface (see Figure 7).

CONCLUSIONS

In this work, a mechanism for the production of a tadpole shaped lesion induced by boiling histotripsy was proposed and investigated. Boiling bubbles were produced in a localised heated region and cavitation clouds were subsequently induced ahead of the expanding bubble. This process was repeated and eventually resulted in a tadpole shaped lesion. A simplified numerical model describing the scattering of the incident ultrasound wave by a vapour bubble was developed to help interpret the experimental observations. Together with the numerical results, these observations suggest that the overall size of a lesion generated by boiling histotripsy is dependent upon the spatial extent of (a) the heated region at the HIFU focus and (b) the backscattered ultrasound wave by the original vapour bubble. Future work will be focused on the prediction of the size of a mechanically induced lesion as well as the comparison of *ex*-and *in vivo* PCD data and induced mechanical injuries with the gel phantom at a given HIFU exposure setting.

Acknowledgments

This work was supported and funded by Department of Mechanical Engineering, University College London. The authors declare that there is no conflict of interest.

REFERENCES

Allen S and Hall T. Real-time MRI feedback of cavitation ablation therapy (histotripsy). J Ther Ultrasound 2015;3: O89.

Aubry JF, Pauly KB, Moonen C, ter Haar G, Ries M, Salomir R, Sokka S, Sekins KM, Shapira Y, Ye F, Huff-Simonin H, Eames M, Hananel A, Kassell N, Napoli A, Hwang JH, Wu F, Zhang L, Melzer A, Kim YS, Gedroyc WM. The road to clinical use of high-intensity focused ultrasound for liver cancer: technical and clinical consensus. J Ther Ultrasound 2013;1:1-7.

Banerjee PK. The Boundary Element Methods in Engineering. London: McGraw-Hill; 1994.

Canney MS, Khokhlova VA, Bessonova OV, Bailey MR, Crum LA. Shock-induced heating and millisecond boiling in gels and tissue due to high intensity focused ultrasound. Ultrasound Med Biol 2010a;36:250-67.

Canney MS, Khokhlova TD, Khokhlova VA, Bailey MR, Hwang JH, Crum LA. Tissue erosion using shock wave heating and millisecond boiling in HIFU fields. AIP Conf. Proc. 9th Int. Symp. on Therapeutic Ultrasound (ISTU 2009), 24-29 September 2009, Aix- en- Provence, France 2010b;1215:36-9.

Gélat P, ter Haar G, Saffari N. A comparison of methods for focusing the field of a HIFU array transducer through human ribs. Phys Med Biol 2014;59:3139-71.

Gélat P, ter Haar G, Saffari N. An assessment of the DORT method on simple scatterers using boundary element modelling. Phys Med Biol 2015;60:3715-30.

Hallaja IM, Cleveland RO, Hynynen K. Simulations of the thermo-acoustic lens effect during focused ultrasound surgery. J Acoust Soc Am 2001;109:2245-53.

Hall TL, Hempel CR, Wojno K, Xu Z, Cain CA, Roberts WW. Histotripsy of the prostate: dose effects in a chronic canine model. Urology 2009;74:932-7.

Hoogenboom M, Eikelenboom D, den Brok MH, Heerschap A, Fütterer JJ, Adema GJ.

Mechanical high-intensity focused ultrasound destruction of soft tissue: working mechanisms and physiologic effects. Ultrasound Med Biol 2015;41:1500-17.

Khokhlova TD, Canney MS, Khokhlova VA, Sapozhnikov OA, Crum LA, Bailey MR. Controlled tissue emulsification produced by high intensity focused ultrasound shock waves and millisecond boiling. J Acoust Soc Am 2011;130:3498-510.

Khokhlova TD, Hwang JH. HIFU for palliative treatment of pancreatic cancer. J Gastrointest. Oncol 2011;2:175-84.

Khokhlova TD, Wang YN, Simon JC, Cunitz BW, Starr F, Paun M, Crum LA, Bailey MR, Khokhlova VA. Ultrasound-guided tissue fractionation by high intensity focused ultrasound in an in vivo porcine liver model. Proc Natl Acad Sci USA 2014;111:8161-6.

Khokhlova VA, Bailey MR, Reed JA, Cunitz BW, Kaczkowski PJ, Crum LA. Effects of nonlinear propagation, cavitation, and boiling in lesion formation by high intensity focused ultrasound in a gel phantom. J Acoust Soc Am 2006;119:1834-48.

Khokhlova VA, Fowlkes JB, Roberts WW, Schade GR, Xu Z, Khokhlova TD, Hall TL, Maxwell AD, Wang YN, Cain CA. Histotripsy methods in mechanical disintegration of tissue: towards clinical applications. Int J Hyperthermia 2015;31:145-62.

Kreider W, Bailey MR, Sapozhnikov OA, Khokhlova VA, Crum LA. The dynamics of histotripsy bubbles AIP Conf. Proc. 10th Int. Symp. on Therapeutic Ultrasound (ISTU 2010), 9-12 June 2010, Tokyo, Japan 2011;1359:427-30.

Lafon C, Zderic V, Noble M, Yuen J, Kaczkowski P, Sapozhnikov O, Chavrier F, Crum L, Vaezy S. Gel phantom for use in high-intensity focused ultrasound dosimetry. Ultrasound Med Biol 2005;31:1383-9.

Lake AM, Hall TL, Kieran K, Fowlkes JB, Cain CA, Roberts WW. Histotripsy: minimally invasive technology for prostatic tissue ablation in an in vivo canine model. Urology

2008;72:682-6.

Lin KW, Kim Y, Maxwell A, Wang TY, Hall TL, Xu Z, Fowlkes JB, Cain CA. Histotripsy beyond the intrinsic cavitation threshold using very short ultrasound pulses: microtripsy. IEEE Trans Ultrason Ferroelectr Freq Control 2014;61:251-65.

Maxwell A, Sapozhnikov O, Bailey M, Crum L, Xu Z, Fowlkes B, Cain C, Khokhlova V. Disintegration of tissue using high intensity focused ultrasound: two approaches that utilize shock waves. Acoustics Today 2012;8:24-37.

Maxwell AD, Cain CA, Hall TL, Fowlkes JB, Xu Z. Probability of cavitation for single ultrasound pulses applied to tissues and tissue-mimicking materials. Ultrasound Med Biol 2013;39:449-65.

Maxwell AD, Wang TY, Cain CA, Fowlkes JB, Sapozhnikov OA, Bailey MR, Xu Z. Cavitation clouds created by shock scattering from bubbles during histotripsy. J Acoust Soc Am 2011;130:1888-98.

Pahk KJ, Dhar DK, Malago M, Saffari N. Ultrasonic histotripsy for tissue therapy. J Phys Conf Ser 2015;581:012001.

Pahk KJ, Mohammad GH, Malago M, Saffari N, Dhar DK. A novel approach to ultrasound-mediated tissue decellularization and intra-hepatic cell delivery in rats. Ultrasound in Med Biol 2016;42:1958-67.

Parsons JE, Cain CA, Abrams GD, Fowlkes JB. Pulsed cavitational ultrasound therapy for controlled tissue homogenization. Ultrasound Med Biol 2006;32**:**115-29.

Pennes HH. Analysis of tissue and arterial blood temperatures in the resting human forearm. J Appl Physiol 1948;1:93-122.

Pierce AD. Acoustics: an Introduction to Its Physical Principles and Applications. New York: McGraw-Hill; 1989.

Pishchalnikov YA, Sapozhnikov OA, Bailey MR, Williams JC, Cleveland R O, Colonius T,

Crum LA, Evan AP, McAteer JA. Cavitation bubble cluster activity in the breakage of kidney stones by lithotripter shockwaves. J Endourol 2003;17:435-46.

Roberts WW, Hall TL, Ives K, Wolf JS, Fowlkes JB, Cain CA. Pulsed cavitational ultrasound: a noninvasive technology for controlled tissue ablation (histotripsy) in the rabbit kidney. J Urol 2006;175:734-8.

Schade GR, Hall TL, Roberts WW. Urethral-sparing histotripsy of the prostate in a canine model. Urology 2012a;80:730-5.

Schade GR, Keller J, Ives K, Cheng X, Rosol TJ, Keller E, Roberts WW. Histotripsy focal ablation of implanted prostate tumor in an ACE-1 canine cancer model. J Urol 2012b;188:1957-64.

Schade GR, Maxwell AD, Khokhlova T, Wang YN, Sapoznikov O, Bailey MR, Khokhlova V. Boiling histotripsy of the kidney: preliminary studies and predictors of treatment effectiveness. J Acoust Soc Am 2014;136:2251.

Simon JC, Sapozhnikov OA, Khokhlova VA, Wang YN, Crum LA, Bailey MR. Ultrasonic atomization of tissue and its role in tissue fractionation by high intensity focused ultrasound. Phys Med Biol 2012;57:8061-78.

Simon JC, Sapozhnikov OA, Wang YN, Khokhlova VA, Crum LA, Bailey MR. Investigation into the mechanisms of tissue atomization by high-intensity focused ultrasound. Ultrasound Med Biol 2015;41:1372-85.

Soneson JE. A user-friendly software package for HIFU simulation. AIP Conf Proc 8th Int Symp on Therapeutic Ultrasound (ISTU 2008), 10-13 September, 2008, Minneapolis, United States 2009;1113:165-9.

Styn NR, Wheat JC, Hall TL, Roberts WW. Histotripsy of vx-2 tumor implanted in a renal rabbit model. J Endourol 2010;24:1145-50.

Tavakkoli J, Birer A, Arefiev A, Prat F, Chapelon JY, Cathignol D. A piezocomposite shock

wave generator with electronic focusing capability: application for producing cavitation-induced lesions in rabbit liver. Ultrasound Med Biol 1997;23:107-15.

ter Haar G, Coussios C. High intensity focused ultrasound: physical principles and devices. Int J Hyperthermia 2007;23:89-104.

Vlaisavljevich E, Kim Y, Allen S, Owens G, Pelletier S, Cain C, Ives K, Xu Z. Image-guided non-invasive ultrasound liver ablation using histotripsy: feasibility study in an in vivo porcine model. Ultrasound Med Biol 2013;39:1398-409.

Vlaisavljevich E, Lin KW, Maxwell A, Warnez MT, Mancia L, Singh R, Putnam AJ, Fowlkes B, Johnsen E, Cain C, Xu Z. Effects of ultrasound frequency and tissue stiffness on the histotripsy intrinsic threshold for cavitation. Ultrasound Med Biol 2015a;41:1651-67.

Vlaisavljevich E, Lin KW, Warnez MT, Singh R, Mancia L, Putnam AJ, Johnsen E, Cain C, Xu Z. Effects of tissue stiffness, ultrasound frequency, and pressure on histotripsy-induced cavitation bubble behavior. Phys Med Biol 2015b;60:2271-92.

Vlaisavljevich E, Maxwell A, Warnez M, Johnsen E, Cain CA, Xu Z. Histotripsy-induced cavitation cloud initiation thresholds in tissues of different mechanical properties. IEEE Trans Ultrason Ferroelectr Freq Control 2014;61:341-52.

Vlaisavljevich E, Xu Z, Maxwell AD, Mancia L, Zhang X, Lin KW, Duryea AP, Sukovich JR, Hall TL, Johnsen E, Cain CA. Effects of temperature on the histotripsy intrinsic threshold for cavitation. IEEE Trans Ultrason Ferroelectr Freq Control 2016;63:1064-77.

Wang YN, Khokhlova T, Bailey M, Hwang JH, Khokhlova V. Histological and biochemical analysis of mechanical and thermal bioeffects in boiling histotripsy lesions induced by high intensity focused ultrasound. Ultrasound Med Biol 2013;39:424-38.

Xu Z, Owens G, Gordon D, Cain C, Ludomirsky A. Noninvasive creation of an atrial septal

defect by histotripsy in a canine model. Circulation 2010;121:742-9.

Zhou Y, Gao XW. Variations of bubble cavitation and temperature elevation during lesion formation by high-intensity focused ultrasound. J Acoust Soc Am 2013;134:1683-94.

Zhu S, Cocks FH, Preminger GM, Zhong P. The role of stress waves and cavitation in stone comminution in shock wave lithotripsy. Ultrasound Med Biol 2002;28: 661-71.

Figure Legends

Figure 1. HIFU experimental set up used for investigating the generation of tadpole shaped lesions resulting from boiling histotripsy.

Figure 2. Simulated acoustic waveforms and peak temperatures at the HIFU focus in the tissue phantom. (a) Acoustic wavefronts with P_{elect} = 200 W (P_+ = 85.4 MPa, P_- = –15.6 MPa at focus). (b) Corresponding peak temperature. The time to reach the boiling temperature of 100ºC is predicted to be 3.66 ms.

Figure 3. Simulated acoustic pressure magnitudes at the HIFU focus using BEM. The contour plots of the incident acoustic pressure (a) without and (b) with a scatterer. The presence of a vapour bubble is indicated by an arrow in (b). The HIFU beam propagates from top to bottom.

Figure 4. A sequence of high speed camera images (a), (b), (d)-(h) obtained in an optically transparent tissue phantom during the single 10 ms HIFU insonation with an acoustic power of 170 W (P_+ = 85.4 MPa; P_- = –15.6 MPa at the HIFU focus). Images were captured at a 15,000 fps. (c) Simulated temperature contour plot at t = 3.4 ms. The HIFU beam propagates from left to right. The vertical lines pass through the HIFU focal point perpendicular to the beam axis. The time at 0 ms corresponds to the start of the HIFU exposure.

Figure 5. Acoustic signal emitted from the HIFU focus in the gel during the single 10 ms HIFU pulse. (a) shows the PCD voltage vs time plot and (b) is the corresponding spectrogram. Acoustic emissions were recorded at a sampling rate of 0.5 GHz. The time at 0 ms represents the start of the HIFU insonation.

Figure 6. High speed images taken over the course of five HIFU pulses. (a) Images acquired of the formation of a boiling bubble during each HIFU pulse (left column). (b) Images captured at the end of each pulse (middle column). (c) Corresponding mechanical damage induced in the gel prior to the arrival of the next HIFU pulse (right column). The HIFU beam

propagates from left to right. The images were captured at a frame rate of 15,000 fps. The vertical lines pass through the HIFU focal point perpendicular to the beam axis.

Figure 7. (a)-(e) high speed images taken over the course of 50 HIFU pulses. (f) is the cross-sectioned lesion after the 50^{th} HIFU pulse and (g) is the same lesion as (f) but with an added dye. An acquisition rate of 1000 fps was used. Images in the left column show bubble activity at the end of each 10 ms HIFU pulse and the right hand column shows the corresponding mechanical damage induced in the gel, which were taken at 1 ms (i.e. 1 frame) before the arrival of the next HIFU pulse. The HIFU beam propagates from left to right. The vertical dashed lines pass through the HIFU focal point perpendicular to the beam axis.

Figure 8. Length measurement (mean ± SD) along the direction of wave propagation and the width along the lateral direction of the "head" and of the "tail" as a function of the number of HIFU pulses. The reference measurement point was at the HIFU focus. Photron FASTCAM Viewer software (Photron, San Diego, CA, USA) was used for the size measurement (24 μm/pixel). Each measurement was repeated five times.

Figure 9. (a) calculated acoustic pressure magnitudes resulting from the scattering of the HIFU field by a boiling bubble. The green arrow indicates the presence of partially shielded acoustic pressure field behind the vapour bubble. The red arrow shows the backscattered pressures. The HIFU beam propagates from top to bottom. (b) a captured high speed image showing a cavitation cluster (indicated by the yellow arrow) in front of and a secondary boiling bubble (indicated by the blue arrow) behind the primary boiling bubble (indicated by the black arrow).

Figure 10. Proposed mechanisms for boiling histotripsy. (a) Shock wave heating. (b) Formation of a primary boiling bubble at the HIFU focus. (c) Rectified growth of a boiling bubble. (d) Production of cavitation clouds (indicated by the green arrow) and secondary

boiling bubbles (indicated by the red arrows). (e) Creation of a tadpole-shaped lesion resulting from boiling histotripsy.

Figure 11. The sum of the incident and the backscattered acoustic pressure magnitudes from a vapour bubble with a diameter of (a) 100 μm, (b) 200 μm, (c) 300 μm and (d) 500 μm. The HIFU beam propagates from top to bottom.

Tables

Table 1. Composition of 50 mL gel with 7% concentration of BSA. APS = ammonium persulfate. TEMED = tetramethylethylenediamine. TRIS = tromethamine.

Components	**Quantity**	**Percent (%)**
Degassed and de-ionised water	35.805 mL	71.61
BSA	3.5 g	7
1 M TRIS	5 mL	10
40% Acrylamide	8.75 mL	17.5
10% APS	0.42 mL	0.84
TEMED	0.025 mL	0.05

Table 2. Properties of tissue phantom used in the acoustic and temperature fields simulations. These values were obtained from Khokhlova et al. (2011).

Properties	**Value**
Speed of sound	1544 m s^{-1}
Mass density	1044 kg m^{-3}
Absorption coefficient at 1 MHz	15 dB m^{-1}
Coefficient of nonlinearity	4.0
Specific heat capacity per unit volume	5.3×10^{6} J $m^{-3}{}^{o}C^{-1}$
Thermal diffusivity	1.3×10^{-7} m^{2} s^{-1}
Ambient temperature	20 ^{o}C

Figure 1

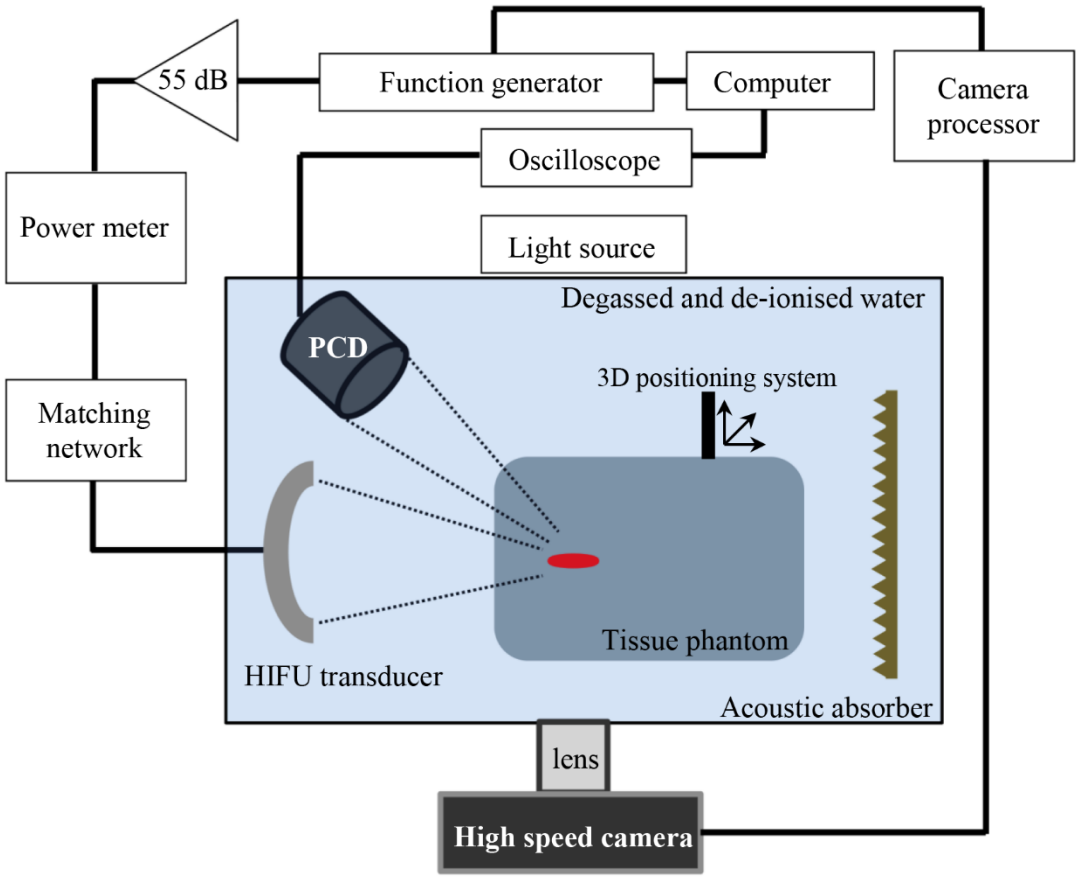

Figure 2

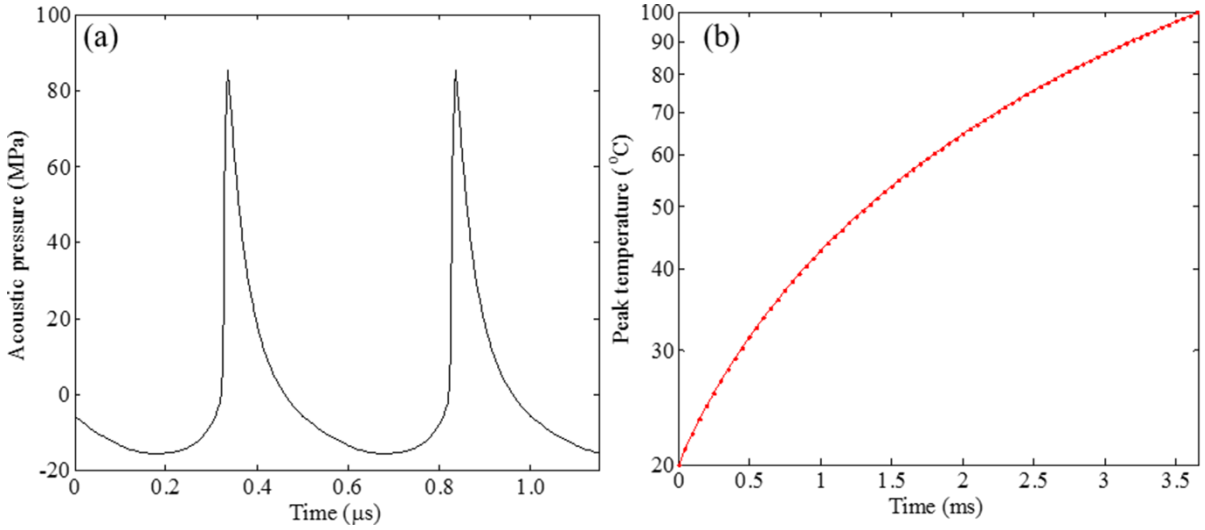

Figure 3

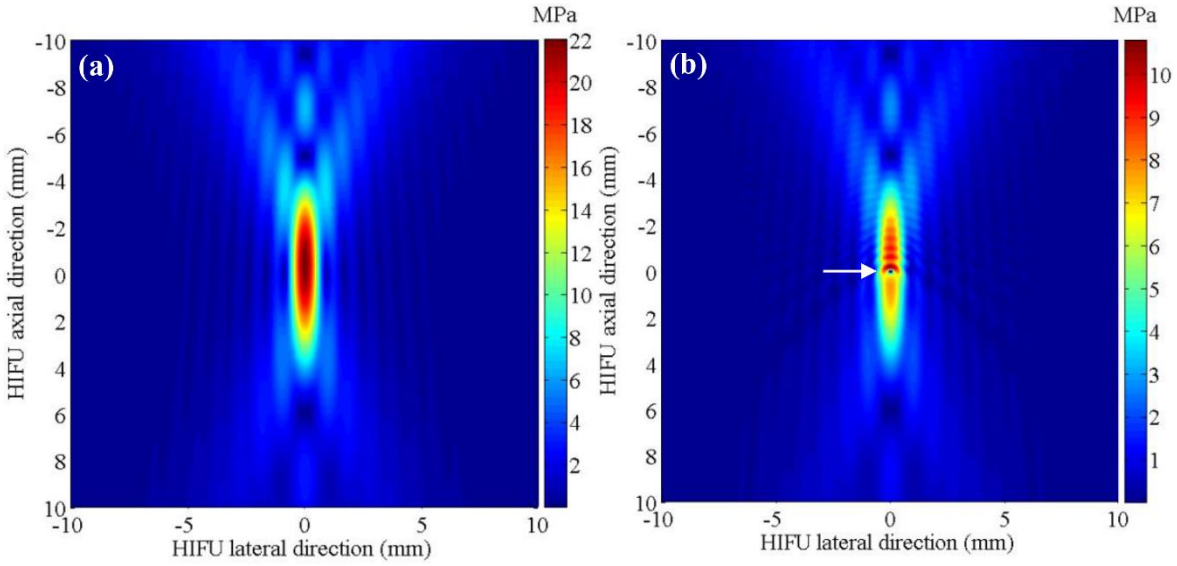

Figure 4

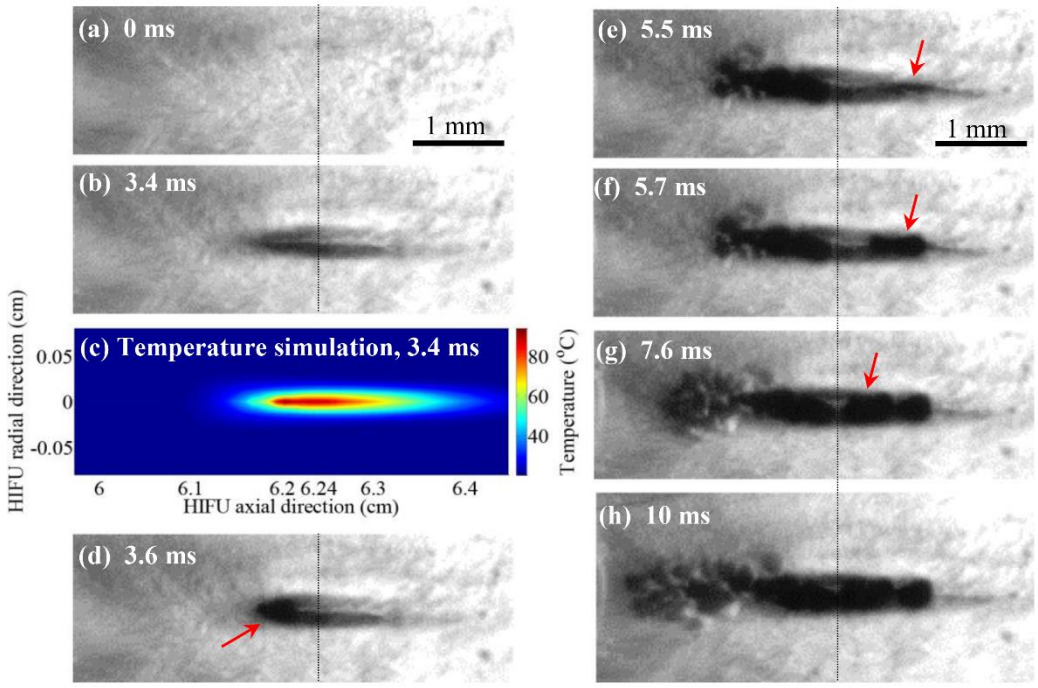

Figure 5

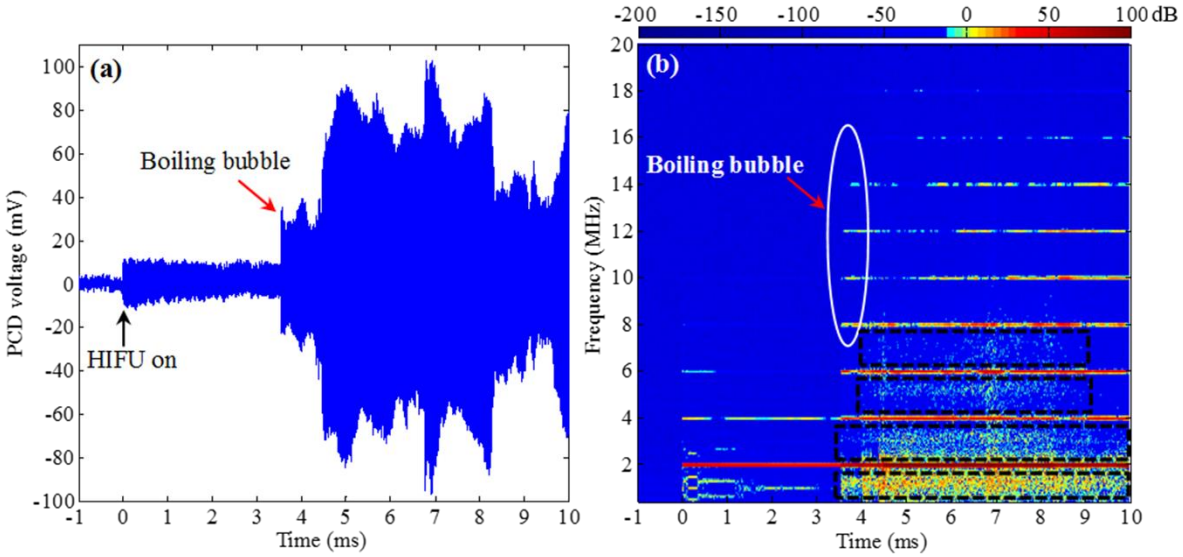

Figure 6

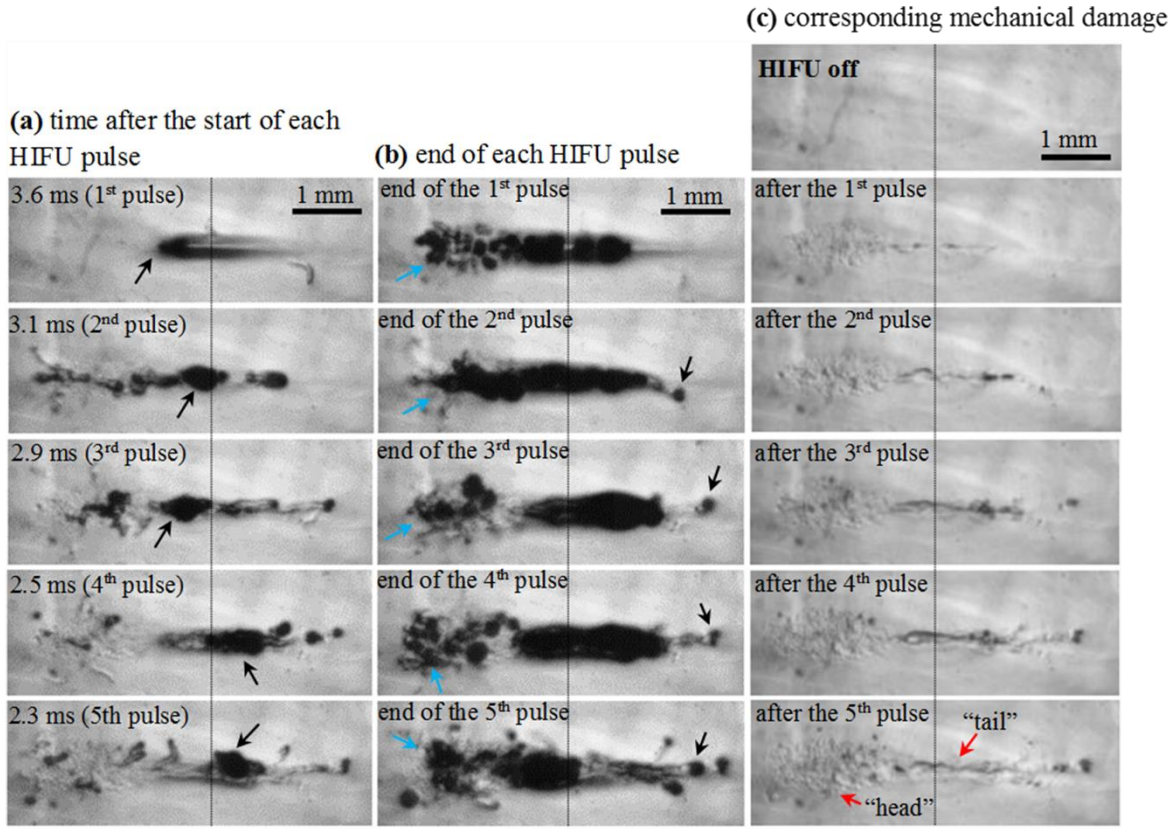

Figure 7

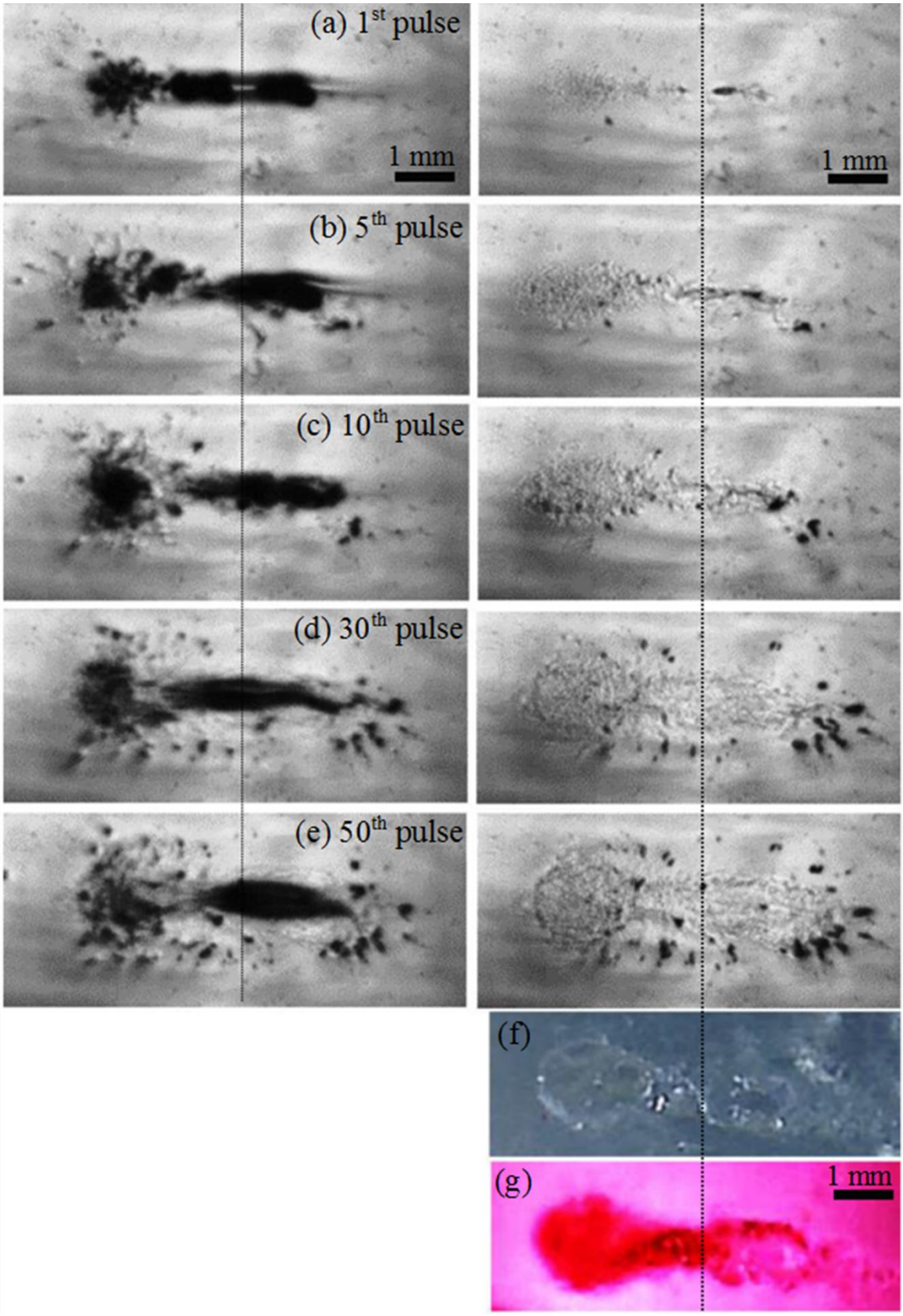
(a) 1st pulse
1 mm
1 mm
(b) 5th pulse
(c) 10th pulse
(d) 30th pulse
(e) 50th pulse
(f)
(g)
1 mm

Figure 8

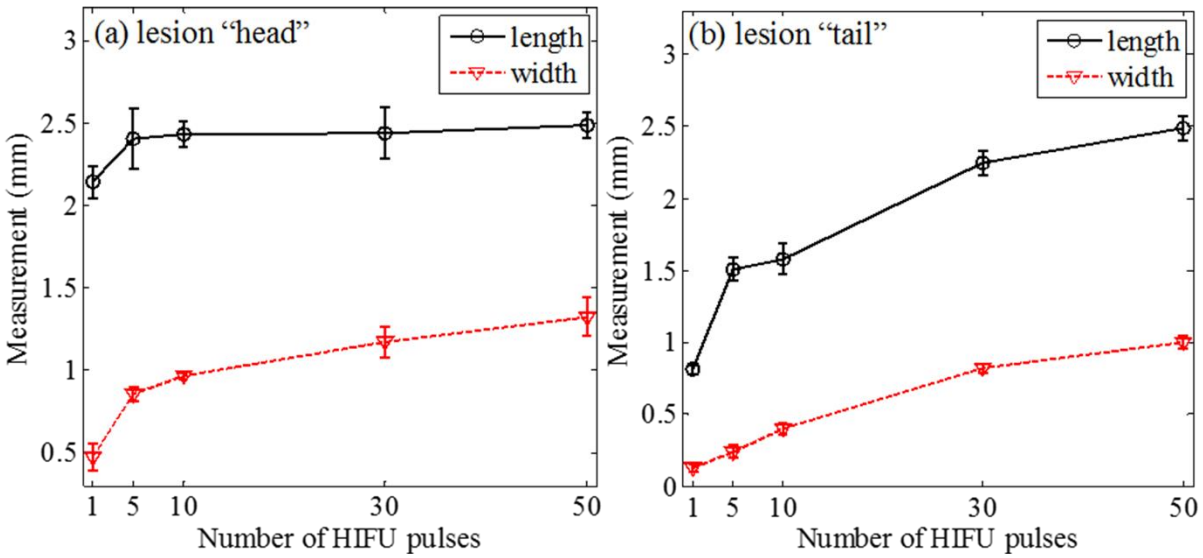

Figure 9

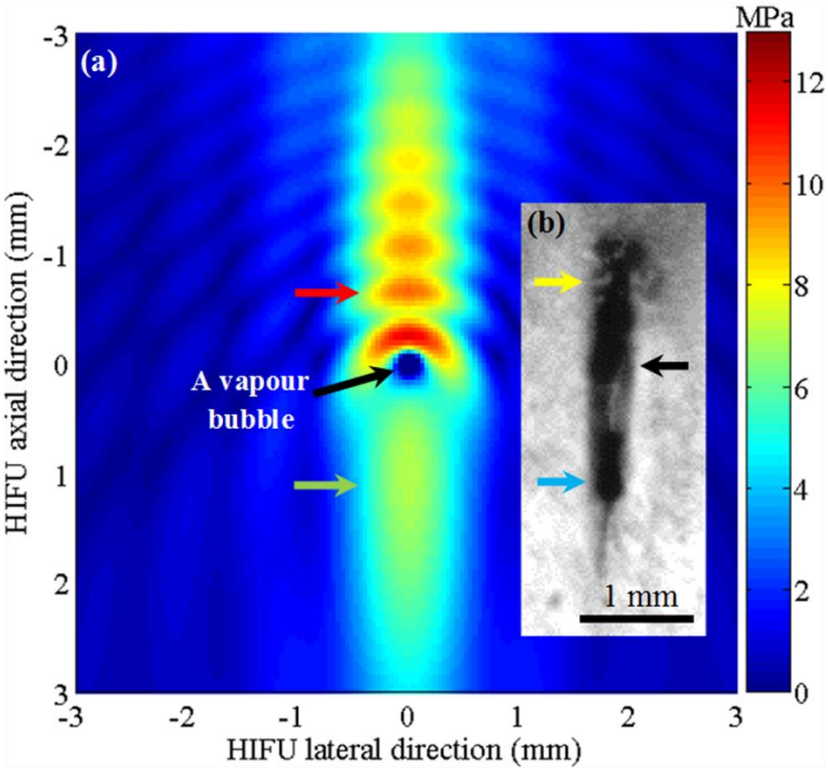

Figure 10

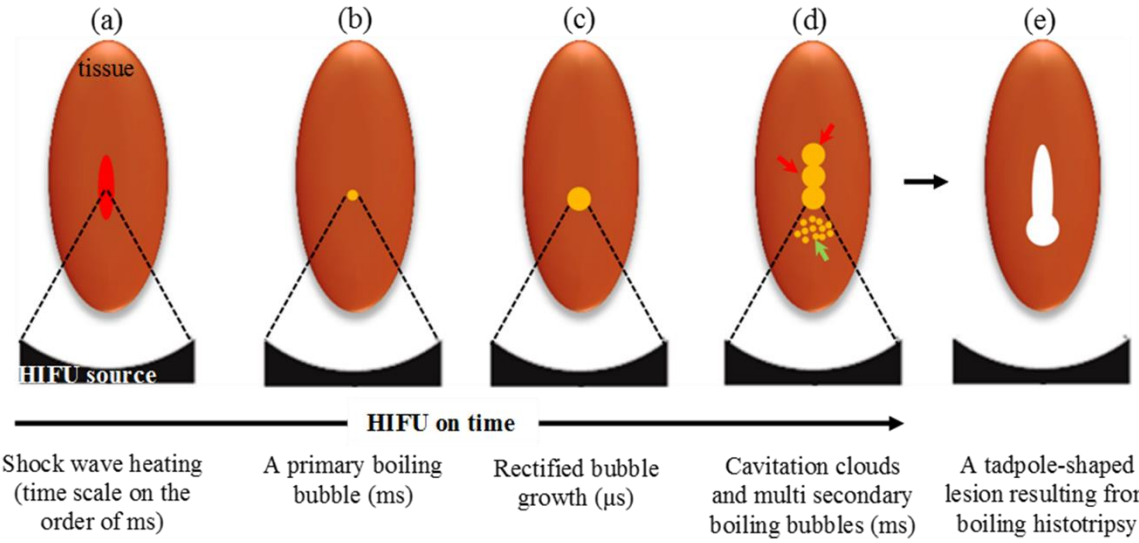
(a)
(b)
(c)
(d)
(e)
tissue
HIFU source
HIFU on time
Shock wave heating (time scale on the order of ms)
A primary boiling bubble (ms)
Rectified bubble growth (μs)
Cavitation clouds and multi secondary boiling bubbles (ms)
A tadpole-shaped lesion resulting from boiling histotripsy

Figure 11

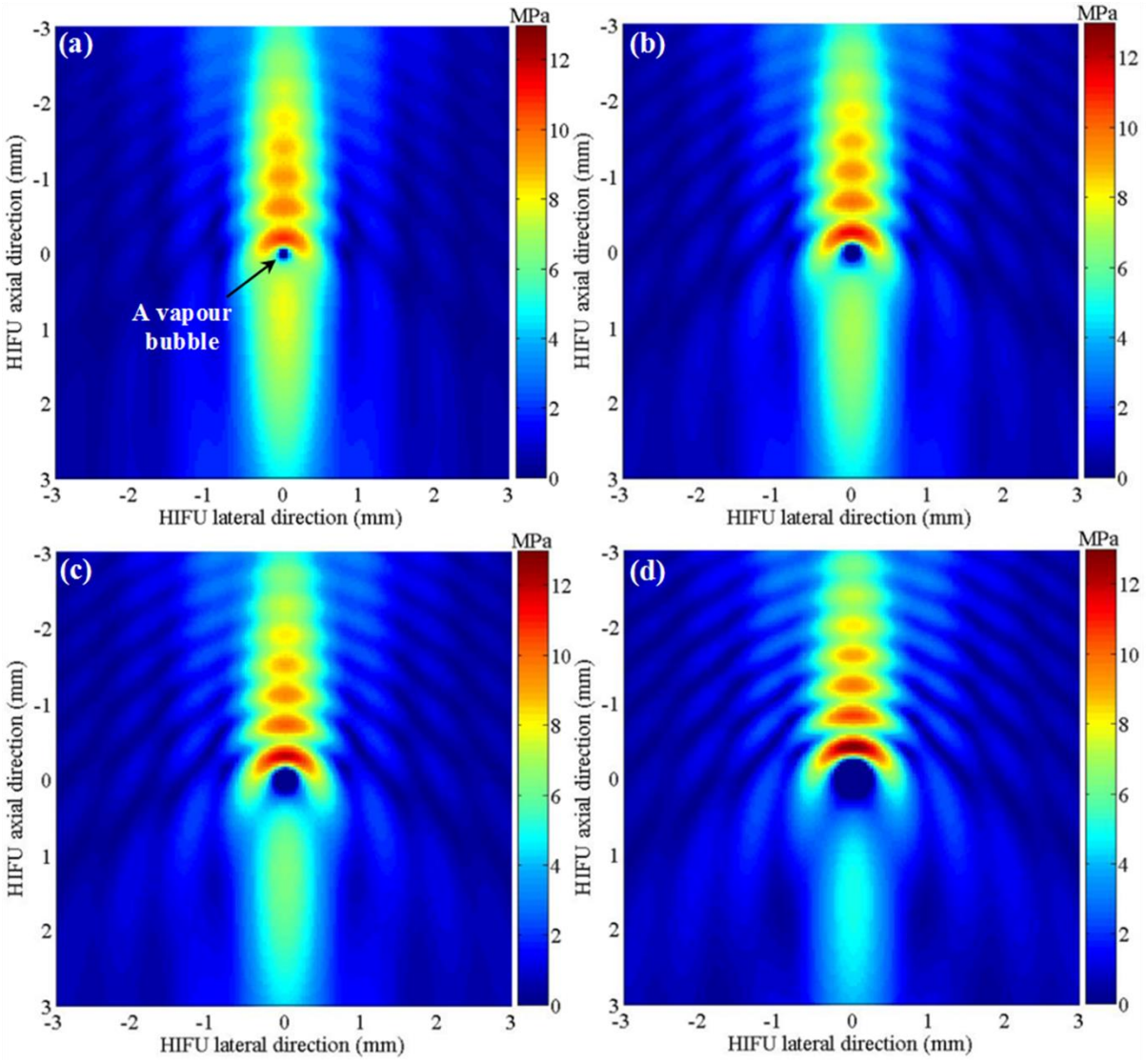
(a)
(b)
(c)
(d)
A vapour bubble
MPa
HIFU axial direction (mm)
HIFU lateral direction (mm)